1 Atomic and Molecular Science

1-1 Breakdown of the One-Electron Orbital Picture for the Xe N-Shell

The one-electron orbital picture enables us to define core-hole states in atoms and molecules. However, inner-shell photoelectron spectra sometimes indicate the breakdown of this simple picture. The most conspicuous examples are the 4p photoelectron lines of the atoms around Z = 54: the photoelectron spectrum of Xe 4p displays only the $4p_{3/2}$ "line" which consists of complicated fine components and a smeared-out $4p_{1/2}$ photoelectron line. A many-body theory succeeded more than 30 years ago in giving a basic description of this feature in the photoelectron spectrum with the following interpretation [1]. The $4p_{1/2}$ photoelectron line is smeared out via the $4p^{-1} \rightarrow 4d^{-2}$ εf super Coster-Kronig (SCK) transition, while the $4p_{3/2}$ core hole is completely spread over the entire spectrum of $4d^{-2}nf$ excitations. Since the one-electron orbital picture for a 4p hole breaks down completely, the concept of a 4p hole is no longer meaningful and the $4p^{-1} \rightarrow 4d^{-2}$ εf SCK transition is to a large extent "virtual". We have succeeded, for the first time, in observing the properties of this virtual SCK transition, by using a very efficient multi-electron coincidence method [2, 3].

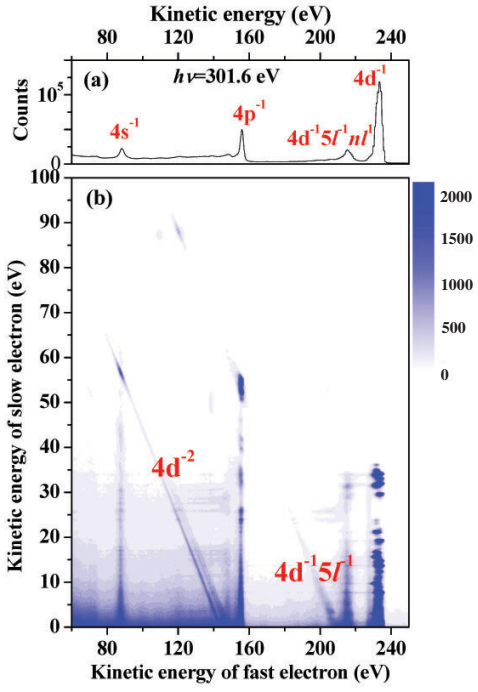

Figure 1
(a) Photoelectron spectrum of Xe obtained at a photon energy of 301.6 eV. (b) Two-dimensional map of all coincidence pairs, represented as a function of the kinetic energies of fast and slow electrons. Coincidence counts in the two-dimensional map are plotted on a linear scale.

A multi-electron coincidence dataset for Xe was accumulated at a photon energy of 301.6 eV [4]. Figure 1(a) shows the photoelectron spectrum in the kinetic energy range of 60 – 250 eV measured at BL-2C, and Fig. 1(b) displays a two-dimensional map showing coincidences between photoelectrons and slower electrons in the energy range of 0 – 100 eV. Several diagonal stripes are observed on the map, which are due to coincidences between photoelectron pairs emitted in double photoionization (DPI) processes. To identify the Xe^{2+} states corresponding to the diagonal stripes, the coincidence counts on the map are projected onto a diagonal axis defined by (fast electron energy) = (slow electron energy). Figure 2 shows the intensity as a function of the total energy of the two electrons for the energy range of 138 – 153 eV, and also the binding energy of Xe^{2+} states. The peaks are allocated to the Xe^{2+} $4d^{-2}$ states associated with DPI from the core orbitals.

It is estimated that the total intensity of the core-core DPI corresponds to around 34% of the 4d single photoelectron intensity. The 4d shake-off mechanism cannot explain the full DPI intensity. The high intensity of DPI supports the theoretical prediction that 4p single ionization provides intensity for $4d^{-2}$ double ionization by mixing through the virtual SCK transition, $4p^{-1} \rightarrow 4d^{-2}$ εf [1]. When the character of the $4d^{-2}$ continuum is governed by this virtual SCK transition from the $4p^{-1}$ continuum, the electron emitted in the Auger transition must be εf. The symmetry of the $4d^{-2}$ εf system is restricted to $^2P_{1/2,3/2}$, as in the intermediate $4p^{-1}$ states; it follows that if orbital angular momentum is conserved, the total orbital angular momentum of the Xe^{2+} $4d^{-2}$ state should be more than 2. This symmetry conservation explains the favored formation, seen in Fig. 2, of the $^1D_2/^1G_4$, $^3F_{2,3}$ and $^3F_4$ components of the Xe^{2+} $4d^{-2}$ state.

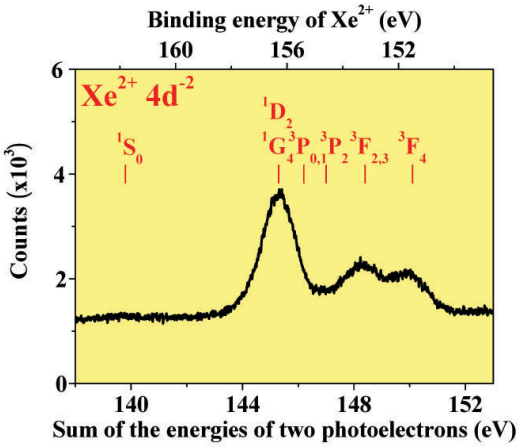

Figure 2
Distributions of the kinetic energy sum for two electrons detected in coincidence, deduced from Fig. 1(b) by integrating the counts along the direction for (fast electron energy) + (slow electron energy) = constant.

Y. Hikosaka[1], P. Lablanquie[2], F. Penent[2], T. Kaneyasu[1], E. Shigemasa[1], J.H.D. Eland[3], T. Aoto[4] and K. Ito[4] ([1]IMS, [2]LCP-MR, [3]PTCL, [4]KEK-PF)

References

[1] G. Wendin and M. Ohno, *Phys. Scr.*, **14** (1976) 148.
[2] J.H.D. Eland, O. Vieuxmaire, T. Kinugawa, P. Lablanquie, R.I. Hall, F. Penent, *Phys. Rev. Lett.*, **90** (2003) 053003.
[3] Y. Hikosaka, T. Aoto, P. Lablanquie, F. Penent, E. Shigemasa and K. Ito, *Phys. Rev. Lett.*, **97** (2006) 053003.
[4] Y. Hikosaka, P. Lablanquie, F. Penent, T. Kaneyasu, E. Shigemasa, J.H.D. Eland, T. Aoto and K. Ito, *Phys. Rev. Lett.*, **98** (2007) 183002.

1-2 Interatomic Coulombic Decay in Ne Dimers

Interatomic Coulombic Decay (ICD) has recently attracted much interest as an efficient mechanism allowing energy transfer from a given site to its environment. It was first predicted theoretically for hydrogen bonded systems ten years ago by Cederbaum *et al.* [1]. Following the first experimental observations [2] and detailed calculations [3], the Ne dimer became the model system for ICD studies.

The process can be schematically depicted in the following way: an inner-valence 2s electron is removed by photoionization from one of the Ne atoms of the weakly bound van der Waals Ne dimer ([Ne---Ne]). The only possible decay channel in the isolated atom is 2p → 2s fluorescence. However, in the presence of a weakly bounded Ne neighbour, a faster inter-atomic process can occur: a 2p electron fills the 2s hole, and simultaneously a 2p electron is ejected from the neighbouring atom via the Coulomb interaction. This process is energetically allowed, and a Ne_2^{2+} dication is then formed, which decays by charge separation into energetic fragment ions:

[Ne---Ne] + hν
→ [$Ne^+(2s^{-1})$ --- Ne] + $e_{photoelectron}$ ***photoionization***
→ [$Ne^+(2p^{-1})$ --- $Ne^+(2p^{-1})$] + e_{ICD} ***ICD***
→ $Ne^+(2p^{-1})$ + $Ne^+(2p^{-1})$ ***Charge separation***

In the present study [4], we have used a very simple and sensitive experimental approach to detect and characterize this ICD process; the observation of fast Ne^+ ions and Ne^+ ion pairs. The experiment was performed at the undulator beam line BL-16B. Ne dimers were produced in a supersonic expansion. The two fragment ions were detected in coincidence using two apparatus: a simple ion filter to reject low energy and thermal ions, and a hemispherical electrostatic analyzer to determine the kinetic energy distribution of the energetic Ne^+ ions.

Figure 3c shows the dimer double photoionization cross section, as deduced from the Ne^+ / Ne^+ coincidence signal. The observation of a threshold near the 2s level and the measured Ne^+ kinetic energy (not shown) demonstrate that double photoionization is dominated by the ICD process, and traces its cross section. Strong resonances are observed above the atomic 2s threshold. A comparison of the ion yield from the atom (Fig. 3a), with the yield of energetic ions from the dimer (Fig. 3b), shows that these resonances originate from the double excitation of one Ne atom in the dimer. Autoionization of these states into the dimer 2s ionization chan-

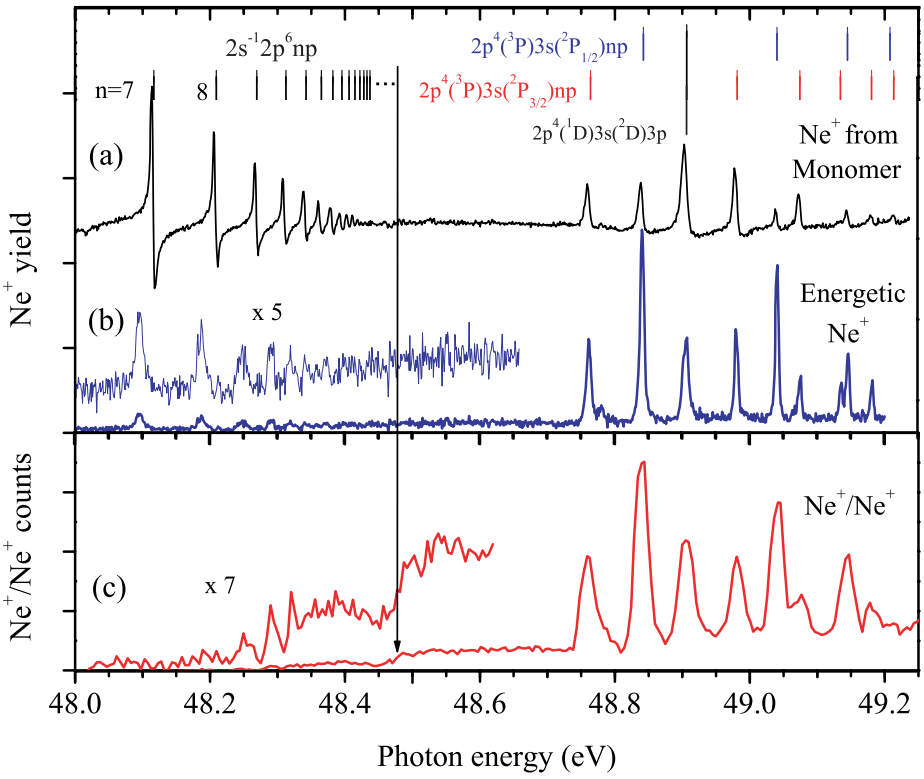

Figure 3
(a) Yield of Ne^+ ions originating from ionization of Ne atoms. (b) Yield of Ne^+ ions with kinetic energies greater than 1 eV, detected using the ion filter. (c) Ne^+ / Ne^+ coincidence yield observed with 20 meV photon resolution; 4 meV resolution was used for (a) and (b).

nel is at the origin of the resonant character of the ICD process. Below the 2s threshold, energetic Ne^+ ions are also observed near the location of the atomic Ne $2s^{-1}$ np resonances (Fig. 3a and 3b). They are usually created with a neutral partner and result from a resonant ICD process:

[Ne---Ne] + hν
→ [Ne*($2s^{-1}$) *np* --- Ne] ***photoexcitation***
→ [Ne*($2p^{-1}$) *np* --- Ne^+($2p^{-1}$)] + $e_{resonant\ ICD}$ ***resonant ICD***
→ Ne*($2p^{-1}$) *nl* + Ne^+($2p^{-1}$)

The Σ and Π symmetries of these molecular [Ne*($2s^{-1}$) *np* --- Ne] states were separated using angle-resolved experiments. The observation of the double photoionization threshold at 280 meV below the 2s atomic threshold can be explained by secondary auto-ionization of the Ne*($2p^{-1}$) *nl* fragments released in the resonant ICD process.

T. Aoto[1], K. Ito[1], Y. Hikosaka[2], E. Shigemasa[2], F. Penent[3] and P. Lablanquie[3] ([1]KEK-PF, [2]IMS, [3]LCP-MR)

References

[1] L.S. Cederbaum, J. Zobeley and F. Tarantelli, *Phys. Rev. Lett.*, **79** (1997) 4778.
[2] S. Marburger, O. Kugeler, U. Hergenhahn and T. Möller, *Phys. Rev. Lett.*, **90** (2003) 203401; T. Jahnke, A. Czasch, M. S. Schöffler, S. Schössler, A. Knapp, M. Käsz, J. Titze, C. Wimmer, K. Kreidi, R.E. Grisenti, A. Staudte, O. Jagutzki, U. Hergenhahn, H. Schmidt-Böcking and R. Dörner, *Phys. Rev. Lett.*, **93** (2004) 163401.
[3] S. Scheit, V. Averbukh, H.-D. Meyer, N. Moiseyev, R. Santra, T. Sommerfeld, J. Zobeley and L.S. Cederbaum, *J. Chem. Phys.*, **121** (2004) 8393, and references therein.
[4] T. Aoto, K. Ito, Y. Hikosaka, E. Shigemasa, F. Penent and P. Lablanquie, *Phys. Rev. Lett.*, **97** (2006) 243401.

1-3 Interatomic Resonant Auger Effect in Fixed-Molecule Core-Level Photoemission

For photoemission from a specific atom in a molecule consisting of different elements, inter-atomic resonant Auger decay is expected to contribute coherently to the direct photoelectron intensity at photon energies corresponding to resonances of the neigbouring atom. A multi-atomic form of this resonance effect is seen in the solid-state, and is referred to as multi-atom resonant photoemission (MARPE) [1, 2]. There has long been a controversy about the degree of resonant enhancements to the effect. The phenomenon is considered to be a general one, but it has been hitherto difficult to observe since autoionization of the initially core-excited atom is much more likely than inter-atomic energy transfer. Therefore, even in molecular spectroscopy, the inter-atomic resonant Auger effect has so far only been observed indirectly, by studying non-dipole contributions to the core-level photoelectron yield from freely rotating molecules [3]. We have recently demonstrated in experiments at the undulator beamline BL-2C that the coincidence velocity-mapping technique allows us to study inter-atomic resonant Auger effects in the molecular frame, providing the most detailed picture to date of the dynamics [4].

Figure 4 shows pictorially two different channels for N 1s photoemission from NO molecules; (a-1) and (a-2) depict the inter-atomic resonant Auger channel, and (b) the direct photoemission channel. When the photon energy matches the neighboring atom O 1s → π* resonant energy, excitation of the core-excited π* state can occur [Fig. 4(a-1)]. The excited NO molecules can subsequently decay via the inter-atomic resonant Auger effect, leading to the same final state as in direct N 1s photoemission [Fig. 4(a-2)]. Thus two interfering channels are possible at the resonant energy. For the polarization geometry parallel to the molecular axis, only the direct photoionization channel [Fig. 4(b)] is open for both on- and off-resonant energies due to the dipole selection rules for the O 1s → π* transition.

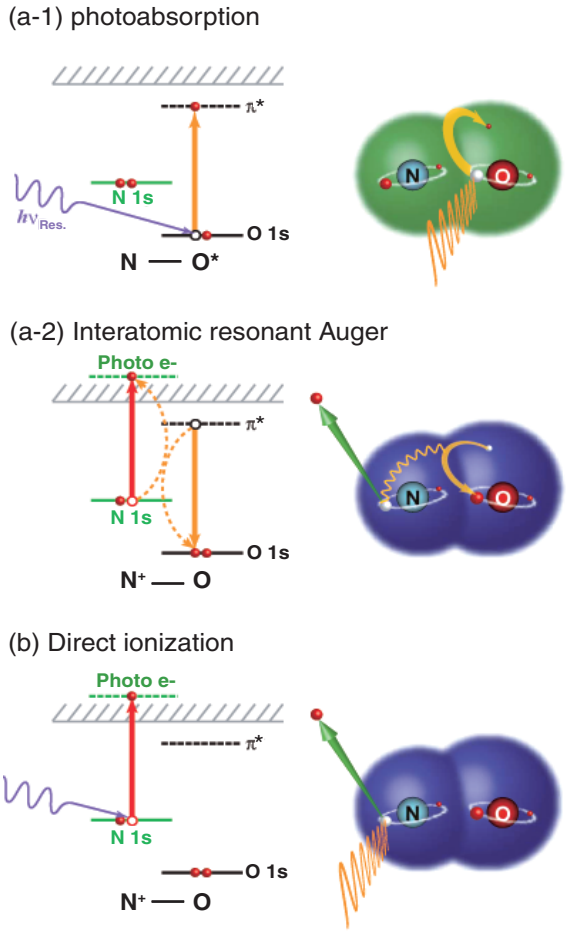

Figure 4
Two different channels for N 1s photoemission from NO molecules; (a-1 and a-2) show the inter-atomic resonant Auger channel and (b) the direct photoemission channel. (a-1) represents photo-absorption by the O atom. (a-2) shows the subsequent inter-atomic resonant Auger decay which leads to emission of the N 1s photoelectron.

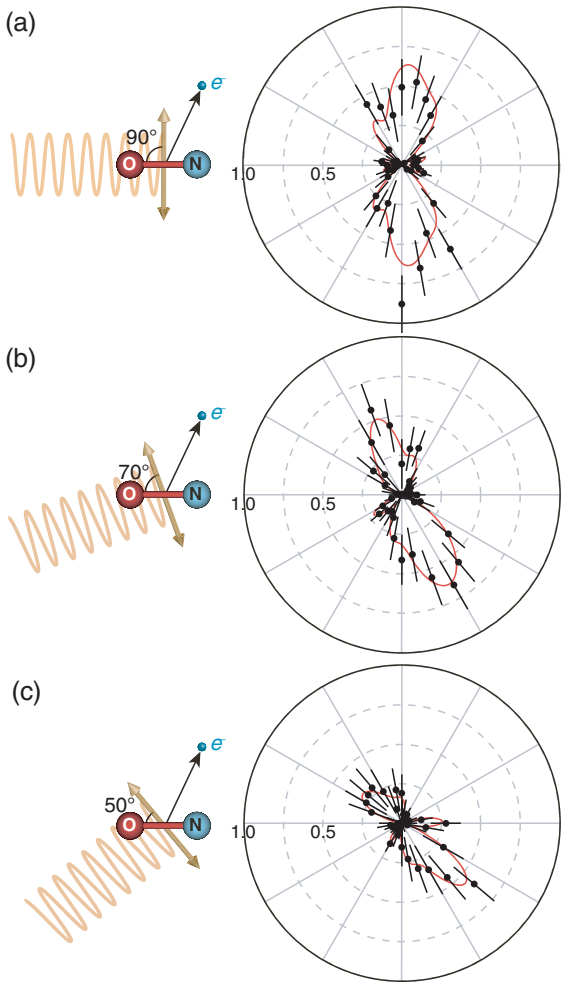

Figure 5
Polar plots of the angular distributions of the N 1s photoelectron intensity enhanced by the inter-atomic resonant Auger process. (a): $\Theta_{ion} = 90°$, (b): $\Theta_{ion} = 70°$, (c): $\Theta_{ion} = 50°$. The plots are obtained from the intensity difference between the on-resonant and off-resonant MF-PADs, and expressed on the same relative scale. The curves are to guide the eyes.

The polar plots in Fig. 5 show resonant enhancement of the N 1s photoelectron intensity for different angles (Θ_{ion}) of the molecular axis to the polarization vector of the incident light. The plots were obtained by subtracting the off-resonance ($h\nu$ = 535.7 eV) N 1s MF-PADs (molecular frame photoelectron angular distributions) from the on-resonance ($h\nu$ = 532.7 eV) MF-PADs. The resonant enhancement was rather small (at most ~ 5%), but the inter-atomic resonant Auger amplitudes clearly appear through interference with the direct photoionization amplitudes in the fixed-in-space NO molecules. The polarization dependence seen in the plots of Fig. 5 reflects the angular dependence of the direct photoionization amplitudes, in which the photoelectrons are preferentially emitted along the electric vector even when modified by the resonant Auger amplitude. Furthermore, there is no contribution from the resonant Auger effect in the direction along the molecular axis, possibly due to the shape and spatial orientation of the photoexcited electronic (π^*) orbital prior to Auger electron emission.

M. Yamazaki, J. Adachi, T. Teramoto and A. Yagishita (KEK-PF)

References

[1] A. Kay, E. Arenholz, S. Mun, F.J. García de Abajo, C.S. Fadley, R. Denecke, Z. Hussain and M.A. Van Hove, *Science*, **281** (1998) 679.
[2] A.W. Kay, F.J. García de Abajo, S.-H. Yang, E. Arenholz, B.S. Mun, N. Mannella, Z. Hussain, M.A. Van Hove and C.S. Fadley, *Phys. Rev. B*, **63** (2001) 115119.
[3] R. Guillemin, O. Hemmers, D. Rolles, S.W. Yu, A. Wolska, I. Tran, A. Hudson, J. Baker and D.W. Lindle, *Phys. Rev. Lett.*, **92** (2004) 223002.
[4] M. Yamazaki, J. Adachi, T. Teramoto and A. Yagishita, *J. Phys. B*, **40** (2007) F207.